JOURNAL OF PROPULSION AND POWER
Vol. 25, No. 5, September–October 2009

Simulation of Combustion Instabilities in Liquid Rocket Engines with Acoustic Perturbation Equations

Jutta Pieringer* and Thomas Sattelmayer†
Technical University of Munich, 85748 Garching, Germany
and
Felix Fassl‡
Astrium, GmbH, 81663 Ottobrunn, Germany

DOI: 10.2514/1.38782

The authors present a new method for predicting combustion instabilities in liquid rocket engines. This method is based on the solution of the linearized governing equations for a three-dimensional combustor geometry in the time domain. The aim of this paper is to show the general feasibility of the approach and to explain the general behavior of the model. The computational domain comprises the combustion chamber itself and the convergent part of the nozzle. The heat release is included via a source term in the linearized energy equation. In the example of the European Aestus engine, it is shown that the model is able to predict the different oscillation modes without any preliminary assumptions about them. An analysis of the influence of the nozzle illustrates that its behavior is automatically included in the approach by design. In comparison to the solution of the full Navier–Stokes equations, the method has the advantage of a much lower numerical cost.

Nomenclature

a	=	velocity of sound
b	=	half-value radius of Gaussian pulse
D	=	diameter
E	=	acoustic energy density
f	=	frequency
I	=	acoustic flux
i	=	imaginary unit
k	=	wave number
L	=	length
M	=	Mach number
n	=	interaction index
$\mathbf{n}$	=	normal vector
p	=	pressure
$\dot{q}$	=	heat release rate
R_{CH}	=	radius of the combustion chamber
r	=	radius (polar coordinates)
T_S	=	oscillation period
t	=	time
u	=	velocity component in direction of the symmetry axis
V	=	volume
x	=	coordinate
Y	=	admittance
Z	=	impedance
α	=	decay/growth coefficient
θ	=	angle (polar coordinates)
κ	=	ratio of specific heats
ρ	=	density
τ	=	delay time
φ	=	phase angle
ω	=	angular frequency

Subscripts

CH	=	combustion chamber
c	=	center
char	=	characteristic
Im	=	imaginary part
N	=	nozzle
num	=	numerical
max	=	maximum
Re	=	real part
sim	=	simulation
theo	=	theoretical
V	=	volumetric

Superscripts

$'$	=	fluctuating quantity
$\bar{}$	=	mean quantity
$+$	=	complex conjugate
$*$	=	nondimensional quantity

Received 28 May 2008; revision received 6 April 2009; accepted for publication 12 April 2009.

*Graduate Engineer, Lehrstuhl für Thermodynamik, Boltzmannstraße 15; pieringer@td.mw.tum.de.

†Professor, Lehrstuhl für Thermodynamik, Boltzmannstraße 15; sattelmayer@td.mw.tum.de.

‡Head of Propulsion Dynamics Team, Space Transportation; felix.fassl@astrium.eads.net.

I. Introduction

HIGH-FREQUENCY combustion instabilities are a dangerous phenomenon in rocket engines. They are responsible for a large number of problems and failures. The phenomenon of combustion instability in liquid and solid rocket engines was discovered in the late 1930s. However, this phenomenon can also arise in gas rockets, afterburners, modern gas turbines, or industrial furnaces.

Efforts to suppress combustion instabilities date back to the 1940s, when baffles and acoustic resonators were used to eliminate the so-called high-frequency resonant burning. Since then, many rocket development programs have been facing the problem of combustion instabilities. Examples are the F-1 engine of the Saturn launch vehicle or the Russian RD-0110 engine of the Soyuz vehicle [1]. Despite the numerous efforts to predict the stability of the various engines by theoretical and analytical methods, most of the stability problems had to be solved by trial and error. This includes expensive full-scale tests. These examples illustrate that the reliable prediction of engine stability is still a challenging problem.

A large amount of literature exits on how to cope with and predict combustion instability. Harrje and Reardon [2], for example,

summarize the state of the art in the United States in the 1970s. A more recent review on combustion instabilities in rocket engines is given by Yang and Anderson [1] in the 1990s, also including the work done in Russia and Europe. Apart from that, several reviews written by Culick [3] have been published. All methods for the prediction of combustion instability are based on the solution of the conservation equations for mass, momentum, and energy. The methods differ in the degree of assumptions and simplifications that are necessary for solving the system of equations. The resulting reduction of complexity of the governing equations leads to a decreasing computational cost. Figure 1 gives an overview of the existing computational methods. The degree of modeling of the methods in Fig. 1 is increased from left to right, whereas the numerical cost decreases from left to right. The basic properties of these different approaches and their importance for rocket stability considerations are summarized in the following sections.

Network models combine the lowest numerical cost and a relatively high degree of modeling. They have become important especially in the stability calculation of gas turbines and industrial furnaces. In the case of rocket stability problems, they are used to model the acoustic behavior of the feed system [4,5]. They supply the boundary condition for the feed system, which is then used in the stability analysis of the whole thrust system [6]. The stability analysis itself is then performed with a different method.

Most methods for the prediction of combustion instability in rocket thrust chambers belong to the second group from the right, termed "Modes Shapes & Harmonic" in Fig. 1. In this case, estimates of the mode shapes as well as the assumption of harmonic oscillations are the basis for the calculation. The early work by Crocco [7] from the 1950s and 1960s reduces the conservation equations to a balance of driving and damping effects. Various authors use principally similar formulations, which differ in their numerical methods.

Solving the linearized conservation equations in the frequency domain without assumptions about the mode shapes leads mathematically to an eigenvalue problem. The use of a frequency-dependant flame model results in a set of equations which cannot be solved by the established mathematical procedures [8,9]. The methods to circumvent this problem developed by Benoit and Nicoud [8] and Nicoud et al. [9] are restricted to low-Mach-number flows. For this reason, further development would be necessary before using them to determine the stability of rocket engines.

Assuming the mode shapes without any restriction to the temporal evolution of the equations reduces the linearized conservation equations to ordinary differential equations. This procedure originates from the mechanical theory of oscillations and is called the Galerkin method. It has been applied for predicting the stability of gas turbines as well as that of rocket engines. This approach also allows one to consider nonlinear wave propagation phenomena by keeping terms of higher order in the acoustic quantities. An overview of the state of the art concerning these nonlinear extensions of the Galerkin method in the 1990s is given by Culick [10]. Recent work by Balasubramanian and Sujith [11] stresses the importance of the correct choice of the underlying oscillation modes.

The direct solution of the linearized governing equations in the time domain is a relatively new field of research. For this approach, neither assumptions about the mode shape nor the behavior of the oscillation amplitudes are required. Nevertheless, the computational effort is low compared to methods which solve the complete conservation equations for mass, momentum, and energy. Pankiewitz and Sattelmayer [12] showed, for the case of the three-dimensional model combustor, that the approach can predict the occurrence of various oscillation modes. By using a nonlinear flame model, limit cycles could be obtained. Their approach was restricted to low-Mach-number flows. This paper deals with the adaptation for its use in rocket combustion chambers.

With increasing computational power, methods that solve numerically the conservation equations for mass, momentum, and energy for reactive flows have gained in importance. These methods have the advantage that the bidirectional interaction between acoustics and fluctuating heat release is implicitly included in the equations. For this reason, there is no need to model this relation. Nonlinear effects are also automatically considered. The disadvantage of these methods is their extremely high computational cost. Furthermore, models for turbulence and combustion are usually needed. In rocket combustion chambers, models for atomization, vaporization, and reaction have to be included. For this reason, approaches that solve the complete set of Navier–Stokes equations for reactive flows numerically are often restricted to two dimensions and/or include restricting models for turbulence and combustion. Additionally, the result for oscillation amplitudes, limit cycles, and oscillation modes depends strongly on the exactness of the models and boundary conditions. First publications by Priem and Breisacher [13] in the 1960s and more recent work by Habiballah et al. [14] show the application of these approaches to rocket combustion chambers.

Nowadays, efforts are made to simulate combustion instabilities by large-eddy simulation (LES) for a further reduction of degree of modeling. In the field of gas turbine instabilities, this approach has already been applied to technically relevant systems. In the field of rocket engines, simulations by LES are still restricted to particular

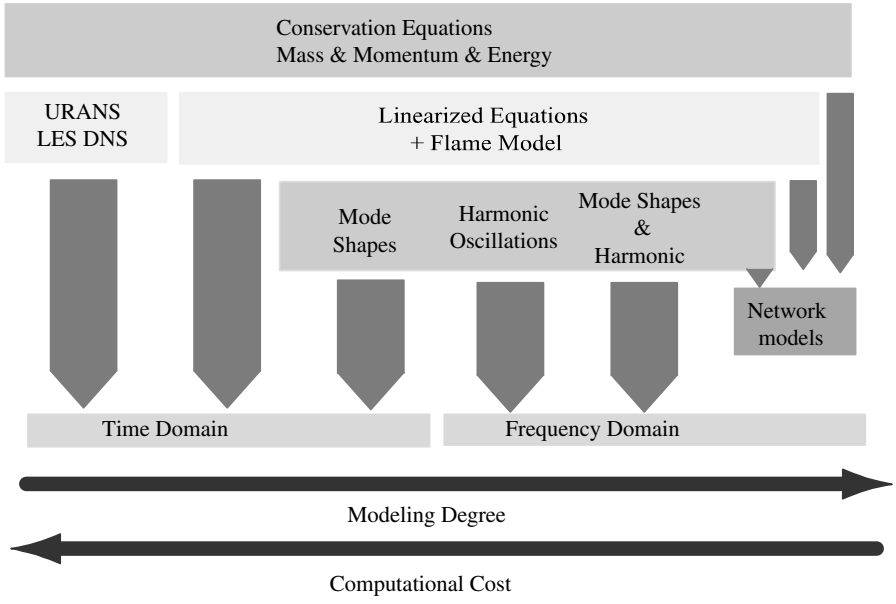

Fig. 1 Simulation methods for predicting combustion instability.

aspects, for example, the response of coaxial injectors to transverse modulation [15]. Further developments will be necessary for the application to complete rocket engines.

This literature review illustrates the existence of a large variety of approaches to predict combustion instability in rocket engines. However, the history of the development of rocket engines shows that, despite this large variety of methods, the reliable prediction and avoidance of combustion instabilities is still a challenging problem. On the one hand, this is partly due to the missing physical models concerning the flame behavior. Additionally, the high degree of modeling concerning acoustic mode shapes of most methods can be held responsible for the lack of reliability. On the other hand, the solution of the complete set of conservation equations for mass, momentum, and energy is numerically too expensive. Consequently, even in this case, restricting assumptions must be made. In some cases, the expression "complete solution" is no longer justified.

This paper deals with an approach for the computation of combustion instabilities in liquid rocket engines which is based on the solution of linearized governing equations in the time domain, in the present case of the so-called acoustic perturbation equations. This set of equations is solved for the three-dimensional combustor geometry including the convergent part of the nozzle. Thus, the method is based on the description of the propagation of the acoustic waves and the development of acoustic oscillation modes with three-dimensional shape in the combustor. Results of the method are the acoustic mode shapes present in the combustor, their temporal evolution, and their stability. For the evaluation of the results, it will be referred to acoustic conservation principles. This includes the reduction of the results to one-dimensional acoustic quantities, so that these can be compared to known results of other methods, such as the nozzle admittance theory introduced by Crocco and Sirignano [16] and Bell and Zinn [17].

As mentioned before, this type of method combines the advantages of a relatively low degree of modeling and high computational effectiveness. This means that, in contrast to most methods for the prediction of combustion instabilities, no assumptions about the mode shapes in the combustor are necessary. Nevertheless, the computations can be carried out on a single processor and computation times are relatively low compared to the full solution of the Navier–Stokes equations. To the authors' knowledge, this kind of approach has not yet been applied for the prediction of combustion instabilities in liquid rocket engines. For this reason, this paper will present the general feasibility of the approach and will focus on its concrete realization. Section II describes the general modeling strategy and presents the basics concerning the set of equations, the necessary input data such as mean flow, and the acoustic energy conservation principles valid in the system. Afterward, Sec. III presents the model setup and discusses the properties of the boundary conditions with regard to acoustic energy balancing. Section IV focuses on the results of the simulations and their analysis concerning the driving capacity of the flame. Section V explains the preponderance of transverse modes in the simulation results by an analysis of the role of rocket nozzle.

II. Modeling Strategy

This section first describes the general idea of the new modeling approach. It then describes the set of linearized equations, the acoustic perturbation equations used in this work. As the correct balancing of acoustic sources and damping mechanisms allows one to predict the acoustic stability or instability of the system, the basic relations of the acoustic energy conservation in the rocket combustion chamber are given. These basic relations are then related to the acoustic admittance of the boundary and to the combustion source. These acoustic energy conservation principles will be used later to analyze the behavior of the model.

A. Basic Approach

Combustion instability results from the interaction between the unsteady heat release of combustion and the combustion chamber acoustics. In rocket engines, the flow is accelerated up to very high Mach numbers, reaching sonic conditions at the nozzle throat. The classical approach to include the influence of the nozzle on the acoustics in the combustion chamber is to represent the nozzle by a nozzle admittance boundary condition. The nozzle admittance for liquid rocket engines is, in general, dependant on the oscillation frequency and on the oscillation mode. This is difficult to apply in a time domain method. Consequently, a different approach was chosen in this work. The chosen governing equations, the so-called acoustic perturbation equations, describe the propagation of acoustic perturbation in nonuniform mean flows. For this reason, they can also be applied to represent the propagation of acoustic waves in the convergent part of the nozzle. Thus, the computational domain in this work contains the combustion chamber and the convergent part of the nozzle. This has the advantage that the reflection properties of the rocket nozzle are included in the simulation for all possible oscillation situations by design.

The focus of this paper is to show the general feasibility and the potential of this approach. For the closure of the equation system, a flame model is needed. As many data are available in literature for the standard model proposed by Crocco and Cheng [18], this well-established model was used to describe the behavior of rocket combustion in the present case. Generally, the approach offers the opportunity to use a different flame model, including, for example, nonlinearities.

B. Acoustic Perturbation Equations

Combustion instabilities are characterized by fluctuations of the pressure p, of the velocity vector $\mathbf{u}$, and of the density ρ. The employed modeling approach is based on the direct solution of the linearized governing equations for the fluctuating quantities p', $\mathbf{u}'$, and ρ' in the time domain for a three-dimensional combustor geometry. The linearized Euler equations can be derived from the conservation equations of mass, momentum, and energy by linearization. Their solution consists of vortical, entropy, and acoustic components which propagate and interact in nonuniform mean flows [19]. Acoustic perturbation equations (APEs) are obtained from the linearized Euler equations by source filtering [20] and describe acoustic wave propagation in non-uniform mean flows. In contrast to the linearized Euler equations, APEs do not describe the convection of vorticity and entropy modes [20]. As the focus of this paper lies on a purely acoustic analysis, an APE system for compressible mean flow was chosen as the basis for the present analysis. The APE system, including the combustion source term, reads

$$\frac{\partial p'}{\partial t} + \bar{a}^2 \nabla \cdot \left(\bar{\rho} u' + \bar{\mathbf{u}} \frac{p'}{\bar{a}^2} \right) = (\kappa - 1) \dot{q}'_V \tag{1}$$

$$\frac{\partial \mathbf{u}'}{\partial t} + \nabla(\bar{\mathbf{u}} \cdot \mathbf{u}') + \nabla\left(\frac{p'}{\bar{\rho}} \right) = 0 \tag{2}$$

The local velocity of sound in the ideal gas is $\bar{a} = \sqrt{\kappa(\bar{p}/\bar{\rho})}$ and is therefore generally not constant in the examined geometry. The density fluctuation ρ' is linked to the pressure fluctuation via the linearized isentropic relation $p' = \bar{a}^2 \rho'$. The influence of the flame appears on the right-hand side of Eq. (1) in terms of the volumetric heat release fluctuation $\dot{q}'_V$ with the SI units in Watts per cubic meter. The mean-flow velocity $\bar{\mathbf{u}}$ and the mean-flow density $\bar{\rho}$ are input data for the APE system. The solution of this equation system containing four equations in a three-dimensional case results in the time-dependant description of the acoustic field and therefore in the three-dimensional distribution of the fluctuating pressure p' and the fluctuation velocity components u', v', and w'.

All of the preceding equations are formulated in the time domain. In acoustics, many relations are commonly formulated in the frequency domain. To convert the expressions from the time to the frequency domain, the assumption of harmonic oscillations in time is necessary. For example, the pressure fluctuation in time domain p' is linked to its counterpart in the frequency domain $\hat{p}$ by the expression

$$p' = \hat{p} \cdot e^{i\omega t} \tag{3}$$

The acoustic stability of a system described by linearized governing equations can be judged by the application of acoustic energy conservation principles. The acoustic energy conservation principles are explained in the next section. These will be applied in the analysis of the behavior of the boundary condition in Sec. III, in the discussion about the stability of the combustion chamber in Sec. IV, and in the investigation of the nozzle damping in Sec. V.

C. Acoustic Energy Conservation Principles

Balancing acoustic sources and acoustic damping allows one to predict the acoustic stability or instability of a system. If the system is unstable, the added energy exceeds the removed energy. In the opposite case, it is stable. For a system without internal losses or sources, the change of acoustic energy in the system results only from the transport of acoustic energy over boundaries. The differential conservation equation reads in this case

$$\frac{\partial E}{\partial t} + \nabla \cdot \mathbf{I} = 0 \tag{4}$$

Integrating Eq. (4) over the volume V of the system, applying Gauss's theorem, and integrating over one oscillation period T_S results in Eq. (5) for the change of acoustic energy in the volume V during one oscillation period:

$$\Delta E_V = \frac{E_{v,t} - E_{v,t-T_S}}{T_S} = -\int_S \langle \mathbf{n} \cdot \mathbf{I} \rangle \, \mathrm{d}S \tag{5}$$

The expression $\langle \mathbf{n} \cdot \mathbf{I} \rangle$ in Eq. (5) designates the mean acoustic flux over the boundary of the system in one oscillation period. Depending on the properties of the acoustic system, various expressions can be found in literature for acoustic energy E and flux $\mathbf{I}$. For a homogenous, quiescent medium, the expressions for E and $\mathbf{I}$ result in the well-known formulas from classical acoustics given in Eqs. (6) and (7):

$$E = \frac{p'^2}{2\bar{a}^2\bar{\rho}} + \frac{\bar{\rho}\mathbf{u}'^2}{2} \tag{6}$$

$$\mathbf{I} = p'\mathbf{u}' \tag{7}$$

Morfey [21] derived expressions for E and $\mathbf{I}$ in isentropic potential flows which take a more complicated form than those from classical acoustics. They are given in Eqs. (8) and (9):

$$E = \frac{p'^2}{2\bar{a}^2\bar{\rho}} + \frac{\bar{\rho}\mathbf{u}'^2}{2} + \frac{(\bar{\mathbf{u}} \cdot \mathbf{u}')p'}{\bar{a}^2} \tag{8}$$

$$\mathbf{I} = p'\mathbf{u}' + \frac{p'^2\bar{\mathbf{u}}}{\bar{\rho}\bar{a}^2} + \bar{\rho}(\bar{\mathbf{u}} \cdot \mathbf{u}')\mathbf{u}' + \frac{p'}{\bar{a}^2}(\bar{\mathbf{u}} \cdot \mathbf{u}')\bar{\mathbf{u}} \tag{9}$$

The expressions in Eqs. (8) and (9) were also used by Cantrell and Hart [22] and Zinn [23] to analyze the acoustic energy balance in the case of rocket instability problems. Candel [24] showed that the temporal mean value of these expressions describes the acoustic energy conservation for the flows in nozzles and diffusers. Therefore, the periodic mean of these expressions can be used to examine the acoustic energy conservation on the whole computational domain considered in this paper, namely the combustion chamber and the convergent part of the nozzle.

D. Relation Between Acoustic Admittance and Acoustic Flux

In the present work, acoustic energy is removed from the system by the acoustic flux over its boundaries. These boundaries are commonly described by a so-called admittance. The acoustic admittance is a quantity that is usually used to describe the acoustic properties of a boundary in the frequency domain. It is defined as the nondimensional ratio between the pressure fluctuation $\hat{p}$ and the normal velocity fluctuation $\mathbf{n} \cdot \hat{\mathbf{u}}$ at this boundary, as given in Eq. (10):

$$Y = \bar{\rho}\,\bar{a}\frac{\mathbf{n} \cdot \hat{\mathbf{u}}}{\hat{p}} \tag{10}$$

Generally, the admittance defined by Eq. (10) is a complex quantity. For a slip wall ($\mathbf{n} \cdot \mathbf{u}' = 0$), the admittance takes the value zero, for an open end ($p' = 0$), it reaches infinity. Nonreflecting boundaries have an admittance of unity. A direct relation between acoustic admittance Y and the periodic mean $\langle \mathbf{n} \cdot \mathbf{I} \rangle$ of the acoustic flux over a boundary can be derived for a one-dimensional mean flow and harmonic oscillations. In the following section, it will be assumed that the mean flow has only one nonzero component u in the direction of the symmetry axis x. The normal vector of the considered surface also points in the direction of the symmetry axis. Oscillations are assumed to be harmonic. Generally, the periodic mean of the product of two harmonic quantities g and h can be calculated by the formula given in Eq. (11):

$$\langle g \cdot h \rangle = \tfrac{1}{2}\mathrm{Re}(\hat{g} \cdot \hat{h}^+) \tag{11}$$

The superscript $+$ designates the complex conjugate value. The combination of the preceding assumptions, Eqs. (9) and (11), yield the expression given in Eq. (12) for the periodic mean of the acoustic flux in the normal direction:

$$\langle \mathbf{n} \cdot \mathbf{I} \rangle = \tfrac{1}{2}\Bigg(\mathrm{Re}(\hat{p} \cdot \mathbf{n} \cdot \hat{\mathbf{u}}^+) + \mathrm{Re}(\hat{p} \cdot \mathbf{n} \cdot \hat{\mathbf{u}}^+) \cdot \frac{\bar{u}^2}{\bar{a}^2} + \bar{\rho}\,\bar{u}[\mathrm{Re}(\mathbf{n} \cdot \hat{\mathbf{u}} \cdot \mathbf{n} \cdot \hat{\mathbf{u}}^+)] + \frac{\bar{u}}{\bar{\rho}\bar{a}^2}\,\mathrm{Re}(\hat{p} \cdot \hat{p}^+) \Bigg) \tag{12}$$

Together with the definition of the admittance in Eq. (10), the periodic mean of the acoustic flux in the normal direction can be written as

$$\langle \mathbf{n} \cdot \mathbf{I} \rangle = \frac{1}{2}\frac{|\hat{p}|^2}{\bar{\rho}\,\bar{a}}\{(1 + M^2)\mathrm{Re}(Y) + M|Y|^2 + M\} \tag{13}$$

For the mathematical simplifications, the property of complex numbers $\hat{g} \cdot \hat{g}^+ = |\hat{g}|^2$ is used. A similar derivation for a different definition of the acoustic admittance was given by Zinn [23]. For a quiescent medium, Eq. (13) reduces to Eq. (14):

$$\langle \mathbf{n} \cdot \mathbf{I} \rangle = \frac{1}{2}\frac{|\hat{p}|^2}{\bar{\rho}\,\bar{a}}\,\mathrm{Re}(Y) \tag{14}$$

Equation (14) shows that, in a quiescent medium, the sign of the real part of the admittance determines if the system loses or gains acoustic energy by the acoustic flux over this boundary. A positive sign indicates an acoustic flux into the system, a negative sign out of the system. For a system with mean flow, the situation is more complicated, as can be seen from Eq. (13). Here, the relation between the Mach number M and the real and imaginary parts of the admittance Y define the sign of the acoustic flux. The formulas linking the acoustic admittance to the acoustic flux are the basis for the analysis of the properties of the used boundary conditions in Sec. III.E and of the influence of the nozzle in Sec. V.

E. Relation Between the Conservation Principle and the Rayleigh Integral

The combustion process can add acoustic energy to the system. This fact is usually expressed in terms of the so-called Rayleigh criterion [25], which is a necessary but not sufficient criterion for the amplification of combustion instabilities. The Rayleigh criterion in Eq. (15) states that combustion adds energy to the oscillation if the integral over the combustor volume of the periodic mean of the product of the volumetric heat release oscillation and the pressure fluctuation takes a positive value:

$$\int_V \frac{1}{T_S} \int_0^{T_S} p' \dot{q}'_V \, \mathrm{d}t \, \mathrm{d}V > 0 \tag{15}$$

For the development of a self-excited oscillation, a second condition must be fulfilled. The supply of acoustic energy by the flame must exceed acoustic losses by dissipation or transport of acoustic energy out of the system. If these damping mechanisms are larger than the excitement by the flame, oscillations will be damped. To consider the influence of the flame in the differential form of the acoustic energy balance in Eq. (4), a source term has to be added to this equation. This source term can be derived by considering the source term describing the influence of heat release, for example, in the linearized Euler equations. After combining the linearized energy and the linearized momentum equation and some algebraic manipulations, the energy source term takes the form given in Eq. (16):

$$S_{\mathrm{comb}} = \frac{(\kappa - 1)}{\bar{\rho}\bar{a}^2} \dot{q}'_V \cdot p' \tag{16}$$

For the periodic mean of the energy balance in the volume V, Eq. (16) results in Eq. (17):

$$\langle S_{\mathrm{Comb}} \rangle = \frac{1}{T_S} \int_{t-T_S}^{t} \int_V \frac{(\kappa - 1)}{\bar{\rho}\bar{a}^2} \dot{q}'_V \cdot p' \, \mathrm{d}V \, \mathrm{d}t \tag{17}$$

The acoustic source term in Eq. (17) is proportional to the Rayleigh integral in Eq. (15). This allows the following interpretation of the source term in Eq. (17) and the Rayleigh integral in Eq. (15), respectively. If the heat release fluctuation and the pressure fluctuation are in phase, the Rayleigh integral takes positive values. In this case, the combustion adds acoustic energy to the system. If the value of the integral is negative, then energy is removed from the system and the combustion has damping characteristics. These relations between heat release fluctuations and the acoustic energy conservation principles will be used in Sec. IV.C to discuss the results of the simulations.

III. Model

This section gives an overview of the properties of the modeled European Aestus engine, which is used as an example to demonstrate the capabilities of the presented simulation approach. This description is followed by the assumptions made in the modeling and the details for the numerical solutions. The illustrations include the description of the used boundary conditions and input data, as well as a discussion of the numerical procedures.

A. Engine

The Aestus engine [26] is used as an upper stage engine in Europe's launcher Ariane 5. During the mission, it consumes about 10 tons of the storable propellant combination MMH and NTO. The Aestus thrust chamber is designed for regenerative cooling. Before combustion, the MMH is pressurized into a distribution manifold and then flows through small channels in the chamber wall to ensure the cooling. The MMH then enters the injection head. The propellants are injected through 132 parallel coaxial injection elements. The NTO is injected in the center and the MMH through radially shaped slots around the NTO jet. The propellants are mixed and atomized by the injection elements. The combustion takes place in the combustion chamber, where the combustion temperature reaches about 3000 K at a combustion pressure of 11 bar at the main stage of operation. A combustion efficiency of above 98% is achieved. Once the mixed propellants are burned, they are accelerated up to sonic conditions in the convergent part of the rocket nozzle.

B. Model

The three-dimensional model in the simulation comprises the combustion chamber and the convergent part of the nozzle, as illustrated in Fig. 2. The modeling is based on the following assumptions:

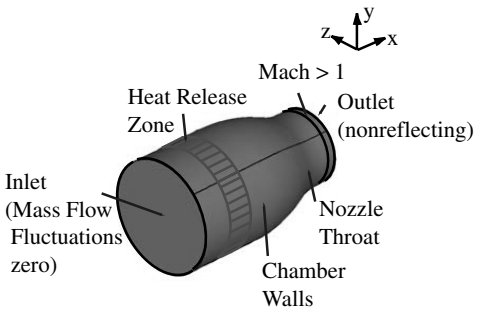

Fig. 2 Model setup with boundary conditions.

1) Combustion chamber and nozzle are filled with hot combustion gas with the properties of the gas at the reference operational point. The reference operational point corresponds to main stage operation. The properties of hot gas in the combustion chamber were calculated by the chemical equilibrium and applications code of Gordon and McBride [27].

2) The combustion chamber walls are assumed adiabatic, although in reality the combustion chamber walls are cooled. This assumption is an acceptable simplification of the reality, as the cooling primarily reduces the temperature of the combustion chamber walls. However, cooling has an insignificant influence on the temperature of the fluid. Additionally, it can be shown that the boundary layers are small compared to the diameter of the combustion chamber.

3) The injected mass flow at the injection head is constant. Consequently, no mass flow fluctuations are considered at this boundary. This assumption is equivalent to decoupling the combustion chamber acoustically from the feed system. This constitutes a strong simplification of the reality. Principally, the modeling approach provides the possibility to include the influence of the feed system by an adequate boundary condition.

4) The nozzle throat sets a well-defined boundary condition for the acoustics: acoustics disturbances cannot propagate upstream once they passed the sonic line.

5) The combustion mainly takes place in the so-called rapid combustion zone (see, e.g., Sutton and Biblarz [28]). This zone is modeled as a disc in the combustion chamber near the injection head.

6) The propagation of disturbances is isentropic. Consequently, entropy waves play no role in this problem and the acoustic wave propagation can be described by the acoustic perturbation equations.

The model makes no assumptions about the behavior of the rocket nozzle and the oscillation modes present in the engine. This constitutes an important advantage in comparison to the classical methods. As the solved linearized governing equations describe the propagation of acoustic disturbances in nonuniform mean flows, mean-flow properties are needed as input for the acoustic simulation. To calculate these, a compressible, two-dimensional, inviscid computational fluid dynamics simulation was carried out. In this simulation, the fluid properties were chosen according to results obtained by the Gordon and McBride code [27] for the reference operation point. In the mean-flow simulation, the combustion chamber, the convergent part of the nozzle, and a section of the divergent part of the nozzle were considered such that the nozzle flow was accelerated up to a Mach number of approximately $M = 1.4$.

As the acoustic code works with nondimensional quantities, the results of the fluid dynamics simulation had to be converted to a nondimensional form by dividing them by reference values. These reference values were chosen to be the following characteristic quantities. As characteristic length L_{char}, the combustion chamber diameter D_{CH} was used. The characteristic velocity u_{char} was defined to be the velocity of sound in the combustion chamber a and as characteristic density ρ_{char} the total density in the combustion chamber. All other characteristic quantities, such as the characteristic time t_{char}, the characteristic frequency f_{char}, the characteristic pressure p_{char}, and the characteristic heat release rate $\dot{q}_{\mathrm{char}}$, can be easily determined from these quantities by Eqs. (18–21):

$$t_{\text{char}} = \frac{L_{\text{char}}}{u_{\text{char}}} \tag{18}$$

$$f_{\text{char}} = \frac{u_{\text{char}}}{L_{\text{char}}} \tag{19}$$

$$p_{\text{char}} = \rho_{\text{char}} u_{\text{char}}^2 \tag{20}$$

$$\dot{q}_{\text{char}} = \rho_{\text{char}} \frac{u_{\text{char}}^2}{L_{\text{char}}} \tag{21}$$

The fluid dynamics simulation and the acoustics simulation are carried out on grids with different geometries and a different spatial resolution. Consequently, the results of the fluid dynamics simulation have to be interpolated to the acoustics grid, such that they are available as input for the acoustics simulation.

Like in many other studies concerning the stability limits of liquid rocket combustion chambers, the heat release model proposed by Crocco and Cheng [18] is used in this work. This model can be expressed in the time domain as given in Eq. (22):

$$\dot{q}'_v = \bar{\dot{q}}_V \frac{n}{\bar{p}_{\text{CH}}} [p'(t) - p'(t-\tau)] \tag{22}$$

The instantaneous pressure fluctuation is $p'(t)$, and $p'(t-\tau)$ is the pressure fluctuation at the time $(t-\tau)$. The model parameters, the interaction index n, and the delay time are constants and do not depend on frequency. In Eq. (22), $\bar{\dot{q}}_V$ is the mean volumetric heat release in the combustion chamber, and $\bar{p}_{\text{CH}}$ is the mean pressure in the combustion chamber. The interaction index n indicates the strength of coupling between heat release and acoustics. The delay time τ can be interpreted as the characteristic time of vaporization.

For hypergolic propellants and coaxial injectors, which are used in the present study, Harrje and Reardon [2] propose the following ranges for τ and n:

$$0.14 \times 10^{-3} \leq \tau \leq 0.20 \times 10^{-3} \text{ s} \tag{23}$$

$$0.6 \leq n \leq 0.8 \tag{24}$$

The values in Eqs. (23) and (24) are empirical values. For determining them, the experimental stability boundaries for various chamber geometries and injector types were compared with the corresponding theoretical predictions.

In the simulation, this model has to be used in the nondimensional form given in Eq. (25):

$$\dot{q}'^*_V = n_{\text{sim}} [p'^*(t^*) - p'^*(t^* - \tau^*)] \tag{25}$$

Nondimensional quantities are marked by $*$. The parameter n_{sim} is a nondimensional input parameter which can be calculated from the formula in Eq. (26):

$$n_{\text{sim}} = n \frac{p_{\text{char}}}{\bar{p}_{\text{CH}}} \frac{\bar{\dot{q}}}{\dot{q}_{\text{char}}} \tag{26}$$

The volumetric mean heat release rate $\bar{\dot{q}}$ was estimated using the following assumptions:

1) For the chemical reaction, the oxidizer and propellant mass flows at the reference operational point are available.

2) The oxidizer is completely consumed during the combustion process.

3) The combustion takes place in a cylindrical zone near the injection head, starting at $x^* = 0.2$ and ending at $x^* = 0.4$. Its diameter corresponds to the diameter of the combustor. The volume of this zone was used to calculate the mean volumetric heat release.

Using these assumptions, the value ranges for n and τ given in Eqs. (23) and (24) result in the following ranges for the nondimensional input parameters n_{sim} and τ^*:

$$0.808 \leq \tau^* \leq 1.213 \tag{27}$$

$$3.756 \leq n_{\text{sim}} \leq 5.008 \tag{28}$$

The heat release fluctuation is a locally varying function of the pressure fluctuation in the heat release zone. At every point in the heat release zone, the heat release fluctuation is a function of the actual pressure fluctuation $p'(t)$ and the past pressure fluctuation $p'(t-\tau)$ at that point. Therefore, the past values up to the time $t - \tau$ must be available during the whole simulation.

C. Analytic Eigenfrequencies

For the definition of the numerical requirements, it is useful to have an idea about the expected oscillation frequencies in advance. A first estimate of the eigenfrequencies of the combustion chamber can be achieved by modeling the rocket combustion chamber as a cylindrical geometry. The analytic estimate is based on the assumption that the combustion chamber can be approximated by a cylinder with the length equal to its diameter. This approximation is known to result in the best correspondence between the estimate and the known eigenfrequencies of the engine. The cylinder is filled with hot combustion gasses and its boundaries are fully reflecting. The analytical solution of this problem (see, e.g., Culick [3]) results in nondimensional frequencies for the analyzed rocket thrust chamber as follows: L1 = 0.50 T1 = 0.59, T1L1 = 0.77, T2 = 0.97, T2L1 = 1.09, R1 = 1.22, and T3 = 1.34. The abbreviation L1 stands for first longitudinal mode, T1 for first transverse mode, T1L1 for first transverse–longitudinal mixed mode, R1 for first radial mode, and so on. These frequencies will also be used to analyze the results of the simulation.

D. Numerical Aspects

To solve the APE system for the three-dimensional combustor geometry, the computational aeroacoustics code PIANO (perturbation investigation of aerodynamic noise) was used. The spatial discretization is realized by a fourth-order dispersion relation preserving scheme (DRP scheme) [29] for curvilinear block-structured grids. Time integration is based on a four-step Runge–Kutta scheme. To suppress nonphysical short wave components, the solution is filtered using a Padé filter [30].

The properties of the DRP scheme and the Padé filter define design rules for the computational grid. The Padé filter should rigorously suppress those frequencies that are not resolved properly by the discretization. Therefore, an ideal filter should have a transfer function with the amplitude one for those frequencies that are well represented by the discretized system, whereas, for all the other frequencies, its amplitude should take the value zero. A closer look at the properties of this filter reveals that the amplitude of its transfer function deviates slightly from the value one even for frequencies that are well represented by the DRP scheme, which leads to numerical damping effects.

To keep these damping effects reasonably small for the frequencies we are interested in, the following aspects were considered by designing the computational grid. Smaller cells lead to a better resolution of higher frequencies. At the same time, smaller cells also lead to a smaller time step for stability reasons. To keep the computational effort reasonably small, cells were chosen as small as necessary and as large as possible. The criterion for the choice of the cell size was the resolution of the T1 mode. The cells were designed such that the amplitude of this mode was independent from the grid resolution. The T2 mode is subject to slight numerical damping. The acoustic transport was resolved up to a Mach number of $M = 0.8$. Mach numbers higher than that are only found on a very small part of the geometry. Thus, the error introduced by this simplification is expected to be negligible.

All simulations were carried out on computers with two dual-core AMD Opterons with 2.4 MHz each and a total random access

memory of 4 GB. The simulation was always done on one of the processors. In this way, up to four cases could be treated on one machine simultaneously. The computational grid consisted of 135,000 cells, and the time step was set to $t^* = 10^{-5}$. The calculation time for the solution of the APE system consisting of four equations was between 4 and 5 days for 40,000 time steps.

E. Boundary Conditions

Boundary conditions play an important part in the energy balance of the acoustics simulation. Therefore, the present section describes the used boundary conditions and their influence regarding the conservation of acoustic energy.

Walls, where the only nonzero component of the mean flow is the one in the parallel direction, are modeled as slip walls. This means that the velocity fluctuations perpendicular to the walls must disappear:

$$\mathbf{n} \cdot \mathbf{u}' = 0 \tag{29}$$

There are no restrictions concerning the acoustic velocity parallel to the walls. In the case of the rocket combustion chamber, all side walls including those of the nozzle were modeled as slip walls.

The slip-wall conditions in PIANO are realized according to the ideas introduced by Tam and Dong [31] by the so-called ghost-point concept. Ghost points are additional virtual points, which introduce additional degrees of freedom in the discretized set of equations. This avoids an overdetermination of the mathematical system and yields more stable solutions. To realize the slip-wall boundary condition, the value of the pressure fluctuation is set at the ghost points. The pressure fluctuation at the ghost point fulfills the linearized momentum equation, such that it yields the condition $\mathbf{n} \cdot \mathbf{u}' = 0$ at the boundary itself. As can be seen from Eq. (7), a slip wall without flow normal to this wall neither removes nor adds acoustic energy to the computational domain.

An inlet-boundary condition is needed for the description of the acoustic behavior of the injection head. The injection head consists of a closed plate with the injection elements in it. As the injection elements take only a small part of the surface of the injection head, it would seem logical to model this boundary as a slip wall. Because of the mapping of the mean-flow velocity field to the grid for the acoustics computation, the mean-flow velocity is nonzero at this boundary. Therefore, this would result in a slip wall with a mean flow over its boundary, which is clearly nonphysical. Mathematically, it can be shown that an acoustic slip-wall boundary with a mean-flow condition would yield an addition of acoustic energy to the acoustic field. This energy addition can be verified by looking at the periodic mean of the acoustic flux over this boundary, described in Eq. (13). The condition $\mathbf{n} \cdot \mathbf{u}' = 0$ for a slip wall reduces Eq. (13) to Eq. (30):

$$\langle \mathbf{n} \cdot \mathbf{I} \rangle = \frac{1}{2} \frac{\bar{u}}{\bar{\rho}\,\bar{a}} |\hat{p}|^2 \tag{30}$$

The acoustic flux adopts only the value zero for $\bar{u} = 0$. In the simulation, this energy addition results in increasing pressure amplitudes with time, even without energy addition by the flame. Therefore, an energetically neutral boundary condition is needed. This can be achieved by setting the mass flow fluctuation to zero. This results in an energetically neutral condition, even for boundaries where mean flow is present. To show this, the mass flow $m = \mathbf{n} \cdot \mathbf{u} \cdot \rho \cdot A$ over a constant cross section A with the normal vector $\mathbf{n}$ will be linearized in Eq. (31) by splitting the velocity $\mathbf{u}$ and the density ρ in its mean and its fluctuation part. The product of the fluctuating quantities $\mathbf{u}'$ and ρ' is small and can therefore be neglected:

$$\begin{aligned} m &= A \cdot \mathbf{n} \cdot \mathbf{u} \cdot \rho = A(\mathbf{n} \cdot \bar{\mathbf{u}} + \mathbf{n} \cdot \mathbf{u}')(\bar{\rho} + \rho') \\ &= \mathbf{n} \cdot \bar{\mathbf{u}}\rho' + \bar{\rho}\mathbf{n} \cdot \mathbf{u}' + \mathbf{n} \cdot \bar{\mathbf{u}}\,\bar{\rho} \end{aligned} \tag{31}$$

The mass flow m can also be split in its mean value and fluctuating part:

$$m = \bar{m} + m' \tag{32}$$

Comparing the second line of Eq. (31) to Eq. (32), the expression for the mass flow fluctuation m' can be identified as

$$m' = \mathbf{n} \cdot \bar{\mathbf{u}}\rho' + \bar{\rho}\mathbf{n} \cdot \mathbf{u}' \tag{33}$$

Setting $m' = 0$ and using additionally the linearized isentropic relation $p' = \bar{a}^2\rho'$, Eq. (33) results in Eq. (34):

$$\mathbf{n} \cdot \bar{\mathbf{u}} \frac{p'}{\bar{\rho}\bar{a}^2} + \mathbf{n} \cdot \mathbf{u}' = 0 \tag{34}$$

Equation (34) means that the combustion chamber is acoustically decoupled from the feed system. Introducing Eq. (34) into the expression for the instantaneous acoustic flux over the boundary in Eq. (9) shows that the acoustic flux over a boundary described by Eq. (34) disappears at any time. Consequently, the injection head can be described by Eq. (34). The implementation of this boundary condition was also realized by the ghost-point concept.

The outlet-boundary condition must describe the acoustic transmission behavior of the rocket nozzle. At the nozzle throat, where the mean flow reaches sonic conditions, acoustic waves cannot propagate upstream anymore. For realizing this nonreflecting behavior, the computational domain was extended into the supersonic region. The governing equations then automatically yield a nonreflecting behavior. The solution in the combustion chamber itself is then independent from the actually applied boundary at the limits of the geometry, which was verified using various possible boundary conditions at the outlet. Finally, the available radiation boundary condition proposed by Tam and Webb [29] was used at the outlet.

F. Initial Condition

As an initial condition, a spherical Gaussian pressure distribution was used. This pressure distribution is defined by the position of its maximum x_c, the pressure amplitude at the maximum $p'_{\max}$, and its half-value radius b:

$$p'(\mathbf{x}, 0) = p'_{\max} \cdot \exp\left[-\ln 2 \frac{(\mathbf{x} - \mathbf{x}_c)^2}{b^2} \right] \tag{35}$$

The pressure distribution introduces a frequency spectrum with a Gaussian frequency distribution. The larger the half-value radius of the pressure distribution, the fewer frequencies are excited. In contrast to that, a Dirac peak would contain an infinite number of frequencies. The extension of the Gaussian pressure distribution was chosen such that all eigenfrequencies mentioned in Sec. III.C can be excited. As the halfway radius, $b^* = 0,1$ was used. The center of the pressure distribution was located in the combustion chamber, with its center off the axis of the chamber.

G. Summary of the Model Properties

The properties and aspects described in the previous sections define a model for the simulation of self-excited combustion instabilities in the time domain that 1) describes the acoustic wave propagation in the mean flow of the combustion chamber and the convergent part of the nozzle, 2) uses the heat release model introduced by Crocco and Cheng [18], 3) makes use of energetically neutral boundary conditions for the side walls and the injection head, 4) allows a removal of acoustic energy by the rocket nozzle, and 5) minimizes the numerical dissipation. This model was used to analyze the development of self-excited combustion instabilities in the Aestus engine.

IV. Results

This section summarizes the properties of the results obtained by the three-dimensional acoustics simulation that is described in Sec. III. Generally, the results give a description of the development of self-excited combustion oscillations in the rocket combustion chamber. Section IV.A gives an overview of the basic features of the results. Section IV.B describes how the stability of the different cases

can be assessed. In Sec. IV.C, the results are analyzed and explained using the Rayleigh integral given in Sec. II.E. Finally, Sec. IV.D summarized the results in the form of a stability map, which is then compared to known descriptions in literature.

A. Results of the Simulations and Their Analysis

The results of the simulation provide the field data of the acoustic variables at different time steps as well as the temporal development of the oscillations at observation points, which have to be specified in advance. This offers the possibility to analyze the shape of the oscillation modes, the frequency spectra, and the stability of the system.

Figure 3 shows the temporal evolution of the (nondimensional) pressure fluctuation p' for a stable and an unstable case. The stable case, which was obtained for an interaction index $n_{\text{sim}} = 1$, possesses a slightly decreasing pressure signal, whereas the unstable case for $n_{\text{sim}} = 3$ yields a growing pressure signal. As some of the observation points might be located in the node of an oscillation mode, the pressure signal must be analyzed at several oscillations points to decide which frequencies and oscillation modes are present in the system.

Figure 4 illustrates the obtained three-dimensional fields for p'. It shows the fluctuating pressure field obtained from two different simulations on the whole combustor geometry at selected time steps. The distribution on the left-hand side of Fig. 4 corresponds to the first transverse mode T1, and the one on the right-hand side to the second transverse mode T2. The deformation of the mode shapes in Fig. 4, that is, the deviation from the ideal theoretical mode shapes of these two modes, indicates that not only one oscillation mode is present in the geometry. Typically, several oscillation modes with varying oscillation amplitudes are superimposed. This can be proved by a frequency domain analysis of the temporal signals at several observation points. Figure 5 shows the frequency content of the obtained time signals for a simulation with $n_{\text{sim}} = 2$ and $\tau^* = 0.7$ in different planes perpendicular to the symmetry axis of the combustion chamber. The corresponding observation points are situated in the pressure antinode of the first transverse mode. The locations given in Fig. 5 refer to the axial distance of these planes from the injection head. All three positions are located on the same straight parallel to the symmetry axis near the oscillation maximum of the first transverse mode T1. The frequency resolution is $\Delta f^* = 0.03$.

Figure 5 shows that several frequencies are always present in the combustion chamber. As the initial condition contains various frequencies, these frequencies must be present in the spectrum. The corresponding amplitudes depend, apart from on the location of the corresponding observation point, on the initial amplitude of this mode and on its damping. In the spectra shown in Fig. 5, the peaks at around $f^* = 0.6$ and $f^* = 0.9$ are the most dominant ones in Fig. 5. They correspond to the first and second transverse mode, respectively. Furthermore, it can be observed that their amplitudes take the largest values in the combustion chamber itself ($x^* = 0.2$) and decrease in the direction of the nozzle (see $x^* = 0.7$). The remaining peaks represent the other possible eigenmodes of the

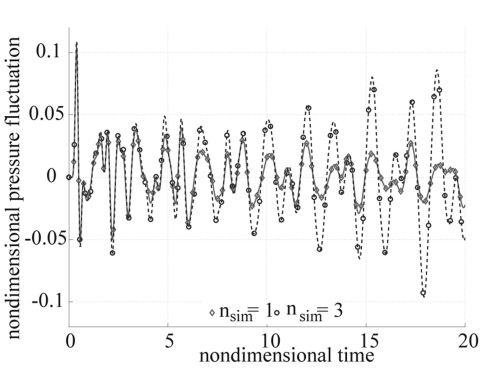

Fig. 3 Temporal development of the oscillation for $\tau^* = 0.7$ in one point and two different values of the interaction index n_{sim}.

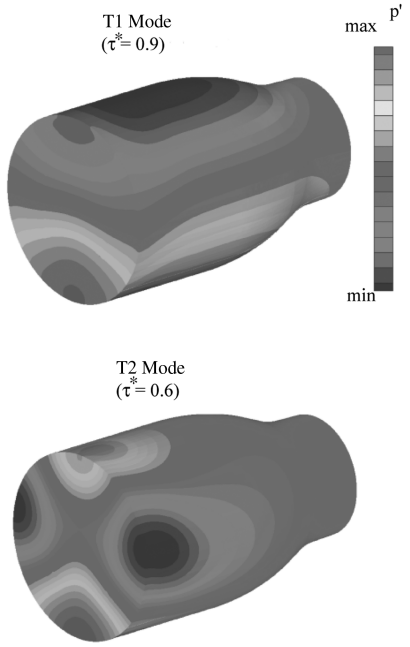

Fig. 4 Field of pressure oscillations for the first and second transverse mode (from the simulations with thermoacoustic heat release model).

combustion chamber. They are all close to the corresponding eigenmodes of a gas-filled cylinder given in Sec. III.C. Generally, only transverse and mixed modes can be observed. Longitudinal modes do not appear in Fig. 5, as they are strongly damped by the nozzle. This effect will be discussed in detail in Sec. V.

B. Determining Stability

A stable system is characterized by declining oscillation amplitudes. Unfortunately, it is not always obvious whether the temporal pressure fluctuation signals grow or decay. Especially near the stability boundaries, interpretation of the results in the time domain is difficult. For this reason, a criterion based on the acoustic energy in the system will be used here to decide about stability or instability. In an acoustically neutral system, the contained acoustic energy neither grows nor decays. This fact can be mathematically derived from Eq. (36):

$$\frac{\partial E}{\partial t} = 0 \Leftrightarrow E = \text{const} \tag{36}$$

In a stable system, the acoustic energy declines with time, whereas it grows in an unstable system. For calculating the acoustic energy in the combustion chamber and the connected convergent part of the nozzle, field data of the fluctuating quantities at selected time steps were used. As the first step, the distribution of acoustic energy in the

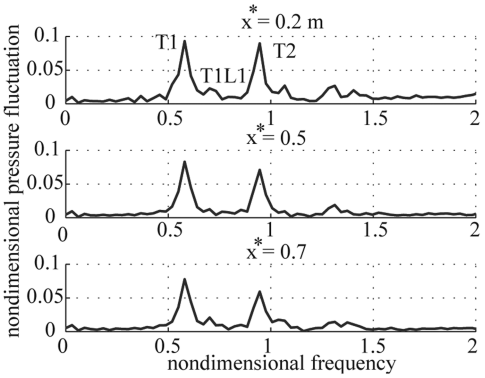

Fig. 5 Frequency spectra at different planes perpendicular to the combustion chamber symmetry axis for $n_{\text{sim}} = 2$ and $\tau^* = 0.7$.

geometry was computed. Integration of the distribution over the volume of the combustion chamber and the convergent part of the nozzle yields the acoustic energy contained in the rocket engine. This value includes the contribution of all modes and frequencies. For this reason, the method can show if the system is stable or not. However, it cannot provide any information about which specific modes are stable or unstable.

Figure 6 shows the temporal development of the acoustic energy in the considered volume for different sets of parameters of the heat release model. The stable cases on the left-hand side of Fig. 6 ($n_{\text{sim}} = 1$) show a monotonic decrease in acoustic energy with time. The unstable cases on the right-hand side of Fig. 6 also start with a decrease of the acoustic energy. This decrease results from the damping of those components of the initial conditions, which will not be amplified by the flame. Once the excitation of the growing modes exceeds the damping, the acoustic energy starts growing. For different time delays, the growth rate is different. This effect is explained by analyzing the Rayleigh integral in Eq. (15) in the next section.

C. Analysis of the Results

The sign of the Rayleigh integral determines whether combustion adds or extracts acoustic energy from the system. A local application of the Rayleigh integral leads to the condition in Eq. (37):

$$\frac{1}{T_S}\int_0^{T_S} p' \cdot \dot{q}'_V \,\mathrm{d}t > 0 \tag{37}$$

This local Rayleigh integral indicates if acoustic energy is produced or destroyed at the considered point. Substituting the heat release fluctuation $\dot{q}'_V$ by the Crocco and Cheng [18] model

$$\dot{q}'_v = \bar{\dot{q}}_V \frac{n}{\bar{p}_{\text{CH}}}[p'(t) - p'(t-\tau)]$$

and assuming sinusoidal oscillations with constant amplitudes of the shape $p'(t) = p_0 \sin(\omega t)$, the local Rayleigh integral can be exploited analytically. Introducing the expression for $\dot{q}'_V$ into Eq. (37) results in

$$\frac{1}{T_S}\bar{\dot{q}}_V \frac{n}{\bar{p}_{\text{CH}}}\int_0^{T_x} p_0 \sin(\omega t) \cdot \{p_0 \sin(\omega t) - p_0 \sin[\omega(t-\tau)]\}\,\mathrm{d}t > 0 \tag{38}$$

Replacing $\omega = 2\pi(1/T_S)$ and carrying out the integration over one oscillation period T_S yields an expression proportional to Eq. (39):

$$\left[\sin\left(\frac{\pi\tau}{T_S}\right)\right]^2 > 0 \tag{39}$$

The expression on the left-hand side of Eq. (39) can take values between zero and one. It can never take negative values. Therefore, a flame described by the heat release model developed by Crocco and Cheng [18] can never have damping properties. The actual value of the expression in Eq. (39) depends on the ratio between the delay time τ and the oscillation period T_S. Consequently, the delay time τ determines the oscillation frequencies at which the Rayleigh integral reaches its maximum. For theses frequencies, the energy supply by the fluctuating heat release also reaches a maximum.

The Rayleigh integral reaches a maximum value for the relations between the delay time τ and the oscillation frequency f_s described by Eq. (40):

$$\tau = \frac{1}{2f_S}(2c-1) \tag{40}$$

The choice of the variable $c \in N$ defines the different periodic solutions of Eq. (39). Introducing the analytical eigenfrequencies of the combustion chamber given in Sec. III.C into the latter equation yields the following values for the delay time τ^*, which will provide optimal amplification of the corresponding modes, summarized in Table 1.

Table 1 Optimal values for the time delay for exciting the corresponding oscillation modes

Mode	Delay time τ^*, $c = 1$	Delay time τ^*, $c = 2$
L1	1.0	3.0
T1	0.85	2.55
L1T1	0.65	1.95
T2	0.51	1.53
R1	0.41	1.23
T3	0.38	1.14

The values for the time delay covered by the parametric study contain the values for the excitation of all modes listed in Table 1. The exploitation of the frequency spectra for several observation points in analogy to Fig. 5 shows that, for all parameter pairs for n and τ^*, the first and second transverse modes are the most dominant ones.

The excitation of these two modes can be analyzed by the value of the Rayleigh integral. The upper part of Fig. 7 shows the amplitudes of the T1 and T2 modes at one point in the combustion chamber as a function of delay time τ^* obtained by the simulation ($n_{\text{sim}} = \text{const}$). The amplitude of the T1 mode reaches its maximum at about $\tau^* = 0.9$ and the T2 mode has a maximum value at about $\tau^* = 0.6$. The lower part of Fig. 7 illustrates the value for the local Rayleigh integral in Eq. (37) for the frequencies of the T1 and T2 modes, also as a function of the delay time. The general behavior of the simulation presented in the upper part of Fig. 7 and the excitation capacity of the flame illustrated in the lower part show an identical behavior. The value zero of the Rayleigh integral means that the flame does not excite a certain mode. For higher values of the delay time, excitation is neither optimal for the T1 nor for the T2 mode. In this case, the

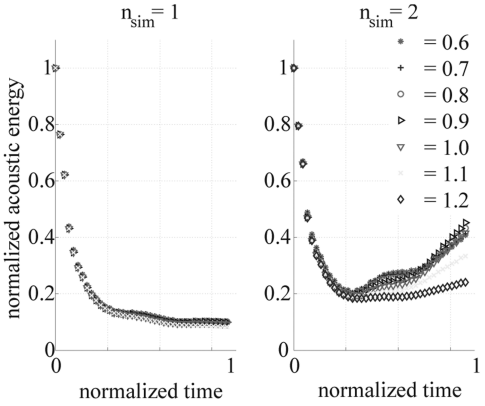

Fig. 6 Temporal development of the acoustic energy in combustion chamber and convergent part of the nozzle for two different values of the interaction index *n*.

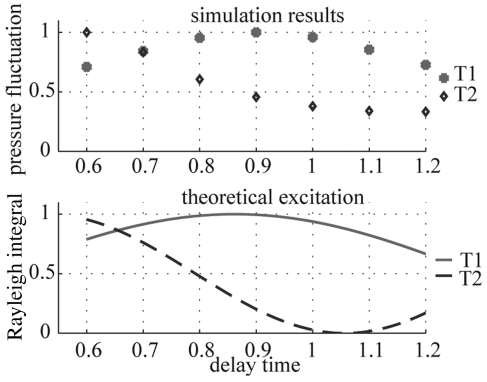

Fig. 7 Comparison of the oscillation amplitudes obtained by the simulation normalized by their maximum value (upper part) and theoretical excitation potential by the Rayleigh integral (lower part) as a function of the delay time.

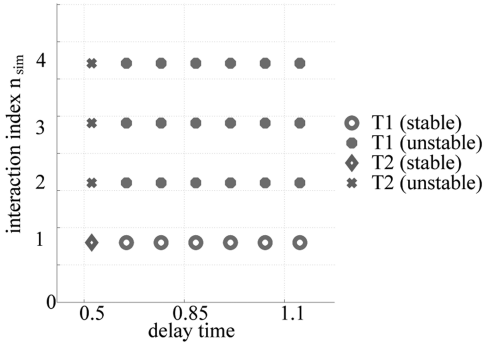

Fig. 8 Stability map.

addition of acoustic energy is lower, but the acoustic losses remain approximately constant. This explains why, in Fig. 6, the growth of acoustic energy is slower for the higher values of τ^*.

D. Stability Map

Results of the simulations were summarized in the form of a stability map. This stability map shows the most dominant mode and its stability as a function of the combustion model parameters, that is, the delay time τ^* and the interaction index n_{sim}. The most dominant mode was determined by the analysis of the corresponding oscillation amplitudes at different observation points. Simultaneously using the information concerning the temporal development of the acoustic energy in the system, the stability of this most dominant mode can be assessed. The stability map is illustrated in Fig. 8.

The stability map makes clear that instability already occurs for small values of the interaction index n. This results from the fact that nozzle damping is the only damping mechanism present in the simulation. Obviously, nozzle damping alone is not sufficient to ensure the stability of the engine in the present case.

In most stability maps found in literature, instability occurs for $n = 0.6$ (corresponding to $n_{\text{sim}} = 3.7$) or higher. In these cases, several damping mechanisms like acoustic absorbers and baffles for the droplet drag are considered. Results published by Mitchell [32], also where only nozzle damping is present, show stability boundaries at very low values of the interaction index. In these results, instability of the T1 mode starts at about $n = 0.25$ ($n_{\text{sim}} = 1.6$). This corresponds approximately to the results illustrated in Fig. 8.

V. Influence of the Nozzle

As shown in the previous paragraphs, the first and second tangential modes T1 and T2 are the two most unstable modes in the investigated rocket thrust chamber. Purely longitudinal modes cannot be observed, whereas mixed modes are present but do not become unstable. These observations will be explained in the next section by analyzing the damping behavior of the rocket nozzle.

A. Classical Nozzle Admittance Theory

The classical method of describing the influence of the nozzle on the acoustic field in the combustion chamber is employing the so-called nozzle admittance. In the work of Crocco and Sirignano [16] and Bell and Zinn [17], the nozzle admittance is defined as the boundary condition imposed by the nozzle to the oscillatory flow in the combustion chamber itself: combustion chamber and nozzle are separated into two zones. The condition to be fulfilled by the acoustic variables at the interface of these two zones is the nozzle admittance. The nozzle admittance Y is expressed as the nondimensional ratio of the axial velocity perturbation $\hat{u}$ to the pressure fluctuation $\hat{p}$ in the nozzle entrance plane, as also defined by Eq. (10).

For the derivation of the linear nozzle admittance, the rocket combustor is divided into two parts: the combustion chamber itself, where combustion takes place and which is characterized by low Mach numbers, and the rocket nozzle, where no heat release occurs and where flow velocities grow and reach choked conditions at the nozzle throat. The gas in the nozzle is treated as ideal. In the divergent part of the rocket nozzle downstream of the throat, the flow is supersonic. Oscillations in the supersonic part of the nozzle have no effect on the conditions upstream of the nozzle throat. Under these assumptions, transient linear equations are derived that describe the wave motion in the rocket nozzle. In the work of Bell and Zinn [17], entropy fluctuations and vorticity waves are excluded from the analysis, whereas the formulation by Crocco and Sirignano [16] accounts for both phenomena. To determine the nozzle admittance condition at the nozzle entrance, the equations are integrated from the nozzle throat up to the nozzle entrance. Both theories employ the following simplifications:

1) In the coordinate transformation, the axial coordinate x is replaced by a steady-state velocity potential, the radial coordinate r by a stream function, and the angle θ designates azimuthal variations.

2) The separation of the variables approach used requires a one-dimensional mean flow, that is, that the angle between the streamlines and the axis of symmetry is small.

3) The time dependence of the fluctuating quantities is harmonic. Using this approach, a solution is found by separation of variables. It requires that the distribution of the axial velocity fluctuation and the pressure fluctuation can be described by the same function in each plane normal to the nozzle axis. This leads to a single value of the nozzle admittance in each of these planes. For a given plane, the admittance is obtained by the numerical integration of the resulting equations. The values for the mean-flow quantities are calculated from the given nozzle contour, which is described by analytical functions, by gas dynamics relations. The analysis provides values for the nozzle admittance depending on the flow properties, the nozzle shape, the oscillation mode and frequency, and, in the case of Bell and Zinn's work [17], also for the decay coefficient α. The nozzle admittance resulting from the theory is a single value valid for the whole nozzle entrance plane and usually a complex valued quantity.

B. Results of the Nozzle Admittance Theory

For a harmonic oscillation with constant amplitude ($\alpha = 0$), the admittance values given in Table 2 are obtained by the Bell and Zinn [17] theory, which has been described earlier. Table 2 shows that the real part $Y_{N,\,\text{Re,theo}}$ as well as the imaginary part $Y_{N,\,\text{Im,theo}}$ of the nozzle admittance takes negative or positive values, depending on the oscillation mode. According to Eq. (13), the sign of the real part of the admittance indicates the direction of the acoustic transport by the intensity $p'\mathbf{u}'$. Negative values of the real part of the admittance reveal that acoustic energy is transported over the nozzle entrance plane from the nozzle into the combustion chambers. Positive values of the real part of the nozzle admittance indicate a loss of acoustic energy from the combustion chamber to the nozzle. The higher the positive value of the real part, the higher are the acoustic losses through the nozzle.

The real part of the nozzle admittance is negative for the first and second transverse mode. In literature, the statement is often found that, for transverse modes, the nozzle has a destabilizing effect. Looking at the complete acoustic flux including the convective transport of acoustic over the nozzle entrance plane, however, usually yields a loss of acoustic energy through the nozzle, also in the case of negative real parts of the acoustic admittance.

The relation between the acoustic transport and the convective transport of acoustic energy can be analyzed by looking at the four contributing terms in the equation for the mean acoustic flux in

Table 2 Real and imaginary part of the nozzle admittance for the Aestus engine evaluated by the theory of Bell and Zinn ($\alpha = 0$) [17]

Mode	$Y_{N,\,\text{Re,theo}}$	$Y_{N,\,\text{Im,theo}}$
L1	1.76	−0.56
T1	−0.22	−0.13
L1T1	1.39	1.00
T2	−0.252	0.096
T2L1	0.95	−0.93

Eq. (13). The first term describes the acoustic flux; the second, third, and fourth terms all describe the convective transport of acoustic energy. For the T1 mode given in Table 2, the first term is destabilizing, as its sign is negative. The second and third term are small compared to the other ones and can therefore be neglected. Consequently, the convective transport is mainly given by the fourth term. It is positive and therefore has a stabilizing influence. The term four is slightly larger than the absolute value of the first term. For this reason, the total influence of the nozzle is stabilizing in this case.

For all modes with a longitudinal contribution, the real part of the admittance given in Table 2 is positive. This means that there are losses of the acoustic energy induced by the rocket nozzle in any case. As a consequence, the acoustic losses for these modes always exceed the acoustic losses for the transverse modes. For the first longitudinal mode L1, the value of the real part of the admittance assumes the largest value. Consequently, for the first longitudinal mode, the damping induced by the nozzle is maximal. This explains why mainly transverse modes can be observed in the calculations explained in Sec. IV.A, although the heat release model has the capacity to excite all modes in the studied frequency range. The same behavior is also observed in reality.

C. Numerical Determination of the Nozzle Admittance

The admittances obtained by the nozzle admittance theory can be verified by comparing them to those derived from the acoustic field in the simulations. The acoustic field in the rocket combustion chamber and in the connected nozzle is given by the temporal evolution of the pressure fluctuation p' and the velocity fluctuation u'. The local nozzle admittance can be extracted from the simulation data by exploiting the information at several observation points in the nozzle entrance plane. The calculation of the local nozzle admittance from the simulation data comprises the following steps:

1) The discrete Fourier-transform is carried out for the time signals of the pressure fluctuation p' and the velocity fluctuation u' normal to the nozzle entrance plane.

2) The amplitudes of $\hat{p}$ and $\hat{u}$ for the frequency of the mode to be studied are extracted.

3) The phase difference φ between the pressure fluctuation and the velocity fluctuation for this frequency is extracted. It is important that the observation point is not located near the nodes of the analyzed mode, because errors might occur during the determination of the phase angle if the amplitude of the signal is too low.

4) The nozzle admittance is calculated from the amplitudes and the phase angle.

The observation points were chosen to be located on two concentric circles in the nozzle entrance plane with the nozzle symmetry axis as center. The inner circle has the radius $r_2 = 0.5R_{\mathrm{CH}}$, and the outer circle the radius $r_1 = R_{\mathrm{CH}}$. As the variation of the nozzle admittance in circumferential direction is insignificant, the mean in circumferential direction will be used in the further argumentation.

The described procedure was carried out for different sets of the parameters n and τ. For these cases, the T1 mode was analyzed concerning the corresponding decay coefficients and the admittance on both circles. The numerical admittance values were then compared to the results obtained by the theory proposed by Bell and Zinn [17] for the respective growth coefficients (a positive value of α means that the oscillation is growing). The growth coefficients in the simulation were determined by curve fitting of the envelope of the pressure signal. Results are summarized in Fig. 9.

The deviations of the numerical values from the theoretical predictions are below 13% for the real parts and below 38% for the imaginary parts. The values from the numerical simulation are generally slightly larger (the absolute value is smaller) than those obtained by the theory. For this reason, the losses induced by the nozzle are slightly larger than those predicted by the theory.

The numerical calculations yield different values for the nozzle admittance on the inner and the outer circle. This is due to effects induced by the two-dimensional mean flow. In contrast to the theory, which is based on the assumption of a one-dimensional mean flow, the mean flow in the simulation is two-dimensional. The outer part of the nozzle, where the streamlines are not parallel to the nozzle axis, therefore shows different values than the inner part.

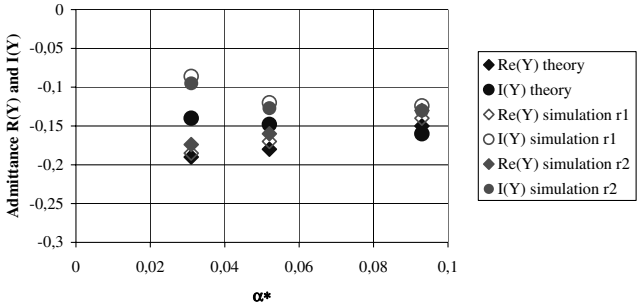

Fig. 9 Nozzle admittances: Comparison between the results obtained by the numerical simulations and the theoretical values obtained by Bell and Zinn's theory [17] for different decay coefficients α.

Apart from those small deviations between theory and numerical results, the agreement between both methods is satisfactory. Consequently, the general behavior of the nozzle can be approximated by the theory developed by Bell and Zinn [17] for analysis purposes. However, results show that the nozzle admittance is a function of the actual oscillation properties. The advantage of the new simulation method in comparison to the use of the classical nozzle theory lies in the fact that it automatically describes the behavior of the nozzle for all oscillation situations, that is, frequencies, modes, and decay coefficients. To use the presented simulation methods, no assumptions about the expected oscillation properties have to be made before starting the calculation.

VI. Conclusions

The prediction of self-excited combustion instabilities is still a problem without satisfactory solution. The known methods suffer from the following restrictions. First, many methods require strong mathematical simplifications of the equations as well as of the physical effects. This high degree of modeling leads to limited reproduction of the underlying reality. Second, methods that solve the complete set of the Navier–Stokes equations are computationally costly. Additionally, they also require models to describe turbulence and combustion. Third, the physical mechanisms leading to combustion instabilities are not completely understood. For these reasons, the existing models are often based on strong simplifications.

In this paper, a new method was presented which requires a relatively low degree of simplifications and is computationally effective. To the authors' knowledge, the numerical solution of the acoustic perturbation equations was not yet used for rocket stability computations, although this approach has substantial advantages. The method is based on the solution of linearized conservation equations on three-dimensional combustor geometries in the time domain. The influence of the fluctuating heat release is modeled by a source term, which allows for a feedback between acoustics and flame behavior. The chosen governing equations, the so-called acoustic perturbation equations, describe the acoustic wave propagation in nonuniform flows. They are based on an ideal gas assumption. The calculation of the wave propagation is carried out in the combustion chamber and the convergent part of the nozzle, which does not require any submodel for the behavior of the nozzle. The present paper shows that this method allows one to simulate self-excited combustion instabilities in the time domain. The resulting oscillation modes can be explained by the application of the so-called Rayleigh criterion. The influence of the nozzle is included by design for all possible oscillation properties.

The results section shows that the output of the model is strongly dependant on the properties of the used heat release model. To show the feasibility of the method in this paper, the well-known, but rather simple, Crocco and Cheng model [18] was used. It was applied to a relatively simple-shaped combustion zone. The extension and shape of this combustion zone must be given and is no result of the

simulation. Nevertheless, this does not restrict the general statement concerning the feasibility of the presented method. A more elaborate flame model would result in a better description of the physics of the interaction between acoustics and rocket combustion.

The presented method has various advantages compared to the classical approaches for the prediction of combustion instabilities. First, no assumption about the oscillation properties, that is, the mode shapes, amplitudes, harmonic oscillations, or decay coefficients is necessary. This information is part of the result of the method. The reflection properties of the nozzle are also automatically contained in the simulation, which avoids the need for preliminary estimates of the nozzle behavior. Furthermore, the solution of the linearized equations is computationally much less costly than the solution of the full Navier–Stokes equations. Finally, the method provides the possibility to include nonlinear flame models or to apply nonlinear boundary conditions to describe, for example, the influence of acoustic absorbers. Coupling with the feed system is also possible by including appropriate boundary conditions at the injection head.

Acknowledgments

This project was funded by Astrium GmbH and the Bayerische Forschungsstiftung in the framework of the project Damping in Thermoacoustical Systems on the Example of the Rocket Engine. This financial support is gratefully acknowledged. We would like to thank the DLR, German Aerospace Center in Brunswick, Germany for providing the numerical tool Perturbation Investigation of Aerodynamic Noise and the members of the Propulsion Dynamics Team of Astrium in Ottobrunn for the valuable discussions.

References

[1] Yang, V., and Anderson, W. (eds.), *Liquid Rocket Engines Combustion Instability*, Vol. 169, Progress in Astronautics and Aeronautics, AIAA, Washington, DC, 1995.

[2] Harrje, D., and Reardon, F., "Liquid Rocket Combustion Instabilities," NASA SP-194, 1972.

[3] Culick, F. E. C., "Combustion Instabilities in Liquid-Fueled Propulsion Systems: an Overview," AGARD CP 450, pp. 1-2–1-73, 1988.

[4] Dordain, J., and Marchetti, M., "Matrices de Transfert de Systèmes Hidrauliques. Etude Théorique et Expérimentale," *La Recherche Aerospatiale*, Vol. 1, No. 1, 1974, pp. 23–35.

[5] Holster, J., and Astleford, J., "Analytical Model for Liquid Rocket Propellant Feedline Dynamics," *Journal of Spacecraft and Rockets*, Vol. 11, No. 3, 1974, pp. 180–187. doi:10.2514/3.62035

[6] DeBenedictis, M., and Ordonneau, G., "Injection Coupled High Frequency Instabilities: Study of Combustion Chamber/Feed System Coupling," *6th International Symposium on Launcher Technologies*, Centre National d'Etudes Spatiales, France, 2005.

[7] Crocco, L., "Theoretical Studies on Liquid-Propellant Rocket Instability," *Tenth Symposium International on Combustion*, The Combustion Inst., Pittsburgh, PA, 1965, pp. 1101–1128.

[8] Benoit, L., and Nicoud, F., "Numerical Assessment of Thermo-Acoustic Instabilities in Gas Turbines," *International Journal for Numerical Methods in Fluids*, Vol. 47, Nos. 8–9, 2005, pp. 849–855. doi:10.1002/fld.886

[9] Nicoud, F., and Benoit, L., and Sensiau, C., and Poinsot, T., "Acoustic Modes in Combustors with Complex Impedances and Multidimensional Active Flames," *AIAA Journal*, Vol. 45, No. 2, 2007, pp. 426–441. doi:10.2514/1.24933

[10] Culick, F. E. C., "Some Recent Results for Nonlinear Acoustics in Combustion Chambers," *AIAA Journal*, Vol. 32, No. 1, 1994, pp. 146–169. doi:10.2514/3.11962

[11] Balasubramanian, K., and Sujith, R. I., "Thermoacoustic Instability in a Rijke-Tube: Non-Normality and Nonlinearity," AIAA Paper 07-3428, 2007.

[12] Pankiewitz, C., and Sattelmayer, T., "Time Domain Simulation of Combustion Instabilities in Annular Combustors," *Journal of Engineering for Gas Turbines and Power*, Vol. 125, No. 3, 2003, pp. 677–685. doi:10.1115/1.1582496

[13] Priem, R., and Breisacher, K., "Nonlinear Combustion Instability Model in Two- to Three-Dimensions," NASA TM-102381, 1989.

[14] Habiballah, M., and Lourme, D., and Pit, F., "PHEDRE-Numerical Model for Combustion Stability Studies Applied to the Ariane Wiking Engine," *Journal of Propulsion and Power*, Vol. 7, No. 3, 1991, pp. 177–191.

[15] Rey, C., and Ducruix, S., and Candel, S., "A Method for the Transverse Modulation of Reactive Flows with Application to Combustion Instability," *Combustion Theory and Modelling*, Vol. 9, No. 1, 2005, pp. 5–22. doi:10.1080/13647830500051950

[16] Crocco, L., and Sirignano, W. A., "Behaviour of Supercritical Nozzles Under Three-Dimensional Oscillatory Conditions," AGARDograph 117, 1969.

[17] Bell, W. A., and Zinn, B. T., "The Prediction of Three-Dimensional Liquid-Propellant Rocket Nozzle Admittances," NASA CR-121129, 1973.

[18] Crocco, L., and Cheng, S., "Theory of Combustion Instability in Liquid Propellant Rocket Motors," Butterworths, London, 1956.

[19] Chu, B.-T., and Kovásnay, L., "Non-Linear Interactions in a Viscous Heat-Conducting Compressible Gas," *Journal of Fluid Mechanics*, Vol. 3, No. 5, 1957, pp. 494–514.

[20] Ewert, R., and Schröder, W., "Acoustic Perturbation Equations Based on Flow Decomposition via Source Filtering," *Journal of Computational Physics*, Vol. 188, No. 2, 2003, pp. 365–398. doi:10.1016/S0021-9991(03)00168-2

[21] Morfey, C. L., "Acoustic Energy in Non-Uniform Flows," *Journal of Sound and Vibration*, Vol. 14, No. 2, 1971, pp. 159–170. doi:10.1016/0022-460X(71)90381-6

[22] Cantrell, R. H., and Hart, R. W., "Interaction Between Sound and Flow in Acoustic Cavities: Mass, Momentum and Energy Considerations," *Journal of the Acoustical Society of America*, Vol. 36, No. 4, 1964, pp. 697–706. doi:10.1121/1.1919047

[23] Zinn, B. T., "Review of Nozzle Damping in Solid Rocket Instabilities," AIAA Paper 72-1050, 1972.

[24] Candel, S. M., "Acoustic Conservation Principles and an Application to Plane and Modal Propagation in Nozzles and Diffusors," *Journal of Sound and Vibration*, Vol. 41, No. 2, 1975, pp. 207–232. doi:10.1016/S0022-460X(75)80098-8

[25] Rayleigh, F. R. S., "The Explanation of Certain Acoustical Phenomena," *Nature*, Vol. 18, No. 455, 1878, pp. 319–323. doi:10.1038/018319a0

[26] "AESTUS-Upper Stage Engine," Information Brochure, Astrium, GmbH, Ottobrunn, Germany, 2001.

[27] Gordon, S., and McBride, B., "Computer Program for Calculation of Complex Chemical Equilibrium Compositions and Applications, II. Users Manual and Program Description," NASA RP-1311, 1996.

[28] Sutton, G., and Biblarz, O., *Rocket Propulsion Elements*, Wiely, New York, 2001.

[29] Tam, C., and Webb, J., "Dispersion Relation Preserving Finite Difference Schemes for Computational Acoustics," *Journal of Computational Physics*, Vol. 107, No. 2, 1993, pp. 262–281. doi:10.1006/jcph.1993.1142

[30] Lele, S., "Compact Finite Difference Schemes with Spectral-Like Resolution," *Journal of Computational Physics*, Vol. 103, No. 1, 1992, pp. 16–42. doi:10.1016/0021-9991(92)90324-R

[31] Tam, C., and Dong, Z., "Wall Boundary Conditions for High-Order Finite-Difference Schemes in Computational Aeroacoustics," *Theoretical and Computational Fluid Dynamics*, Vol. 6, Nos. 5–6, 1994, pp. 303–321. doi:10.1007/BF00311843

[32] Mitchell, C., *Analytical Models for Combustion Instability*, Vol. 169, Progress in Astronautics an Aeronautics, AIAA, Washington, DC, 1995, Chap. 15.

D. Talley
Associate Editor